scientific reports

Check for updates

OPEN

Efficient template free polymerization of continuously porous hybrid conducting polymers for highly stable flexible micro pseudocapacitors

Guldana Zhigerbayeva[1,2], Asset Aliyev[1], Yerbolat Magazov[1,2], Vladislav Kudryashov[2], Salimgerey Adilov[3] & Nurxat Nuraje[1,2]✉

Developing high-performance microscale-energy storage devices is essential for next-generation smart electronics. Hybrid conducting polymers (HCPs) offer a promising solution to address the limitations of traditional conducting polymers, with poor cycling and mechanical stability. Here, we present a novel, template-free bicontinuous microemulsion (BME)-based method of fabricating highly cross-linked, continuously porous PPy-CoO electrodes for micro-pseudocapacitors (MPCs). The bicontinuous structure endows HCPs with tunable functionalities, mechanical flexibility, and efficient ion transport. The synergy between PPy's fast charge transfer and CoO's high charge-storage capacity boosts the electrochemical performance of device, with excellent areal capacitance of 30.58 mF cm^{-2}, energy density of 4.22 μWh cm^{-2}, and power density of 75.97 μW cm^{-2} at 0.2 mA cm^{-2}. The device retains 106% capacitance under 180° bending and 83% capacitance retention after 10,000 cycles in a bent (180°) position. This study demonstrates the BME polymerization approach as a scalable, cost-effective, and versatile strategy for producing multifunctional 3D HCP composites for functional devices.

Keywords Wearable electronics, Micro-pseudocapacitor, Continuously porous, Planar integrated system, Bicontinuous microemulsion

The rising demand for effective, flexible, and lightweight energy storage devices has driven the advancements in materials and fabrication techniques for micro-supercapacitors (MSCs), addressing key limitations of traditional supercapacitors[1–3]. Flexible MSCs, particularly with planar interdigital designs, have received increasing attention as a promising game changer, offering higher energy density, faster charge-discharge cycles, and longer lifetimes[3–5]. This design is suggested as an alternative to sandwiched configurations due to its shorter ion diffusion path, higher electrochemical surface area, and better interaction between the electrode and electrolyte[5]. Moreover, planar MSCs commonly utilize gel-based electrolytes (e.g., PVA/H_2SO_4, PVA/H_3PO_4, PVA/KOH) to prevent electrolyte leakage, making them ideal for portable and wearable applications[6].

The performance of the flexible soft electronics critically depends on the properties of electrode material, electrode-electrolyte interaction, and device design parameters. Moreover, the proven superior electrochemical performance of three-dimensional (3D) porous electrode materials over two-dimensional (2D) thin films in micro-scale energy devices is an essential parameter to consider[7–9]. However, fabricating porous materials with preserved physical and chemical properties of 2D materials is still a big challenge.

Among various materials, conducting polymers (CPs), especially polypyrrole (PPy), have received considerable attention due to their excellent electrical properties, environmental stability, ability to undergo rapid charge-discharge cycles through pseudocapacitive mechanisms, and, most importantly, structural variability and processing flexibility[10–15]. However, despite the advantages of CPs, they suffer from structural degradation and limited long-term stability during repeated electrochemical cycling tests, which hinder their performance in

[1]Department of Chemical & Materials Engineering, School of Engineering & Digital Science, Nazarbayev University, Astana 010000, Kazakhstan. [2]Renewable Energy Lab, National Laboratory Astana, Astana 010000, Kazakhstan. [3]Department of Chemistry, School of Sciences and Humanities, Nazarbayev University, Astana 010000, Kazakhstan. ✉email: nurxat.nuraje@nu.edu.kz

practical applications[12,16]. To overcome existing challenges, hybrid composite conducting polymers (HCPs) are a promising candidate for functional devices with long-term stability. Integration of transition metal oxides (e.g., MnO_2, CoO, Cu_2O, V_2O_5) into conducting polymers is one of the cost-effective solutions[16–23]. Cobalt oxides (CoO, 4292 F g^{-1} and Co_3O_4, 3560 F g^{-1}) are good alternatives to expensive RuO_2 due to their multiple oxidation states, high theoretical capacitance, and low cost[17]. A comparative study by Reddy M. et al. found that CoO outperformed Co_2O_3 and Co_3O_4 in lithium storage applications, exceeding theoretical capacity expectations[24]. However, cobalt oxides commonly suffer from low electrical conductivity and poor surface area, limiting their electrochemical performance[25,26].

Cheng Zhou et al. designed a 3D CoO@PPy hybrid nanowire array on nickel foam with pseudocapacitive performance of 2223 F·g^{-1} and cyclability[25]. However, to the best of our knowledge, no studies have yet been dedicated to microscale interdigital and flexible energy storage devices based on hybrid conducting polymer electrodes of cobalt oxide and polypyrrole.

In this study, we introduce for the first time an advanced template-free approach for the fabrication of continuously porous 3D PPy-CoO electrodes for highly efficient, durable, and flexible micro-pseudocapacitors (MPCs). We designed bicontinuous microemulsion (BME) nanoreactors for one-step, tunable, and controllable fabrication of multifunctional hybrid conducting polymer composites with various microstructures[27]. The proposed approach with a unique interconnected reactor design allows the formation of an open-cell, porous, highly cross-linked polymer network, facilitating efficient ion transport and ensuring the uniform distribution of CoO NPs within the PPy matrix. The porous microstructure of the PPy-CoO electrode controls ion diffusion, allowing better electrolyte ion penetration into the electrode material. The intercalation of proton ions into CoO during highly reversible redox reactions allows the electrode to maintain its capacitance over multiple charge-discharge cycles, which is crucial for the long-term stability of the device.

We systematically investigated the electrochemical and mechanical properties of the PPy-CoO MPCs and demonstrated the superior performance of composite electrodes over pure polypyrrole. Our findings proved that incorporating CoO NPs into the PPy matrix significantly improves both cycling stability and capacitance retention of the device, even under extreme bending conditions, showing the potential possibility of application as a flexible energy storage device.

This paper proposes a new perspective application of the BME-based fabrication approach for the development of highly efficient multifunctional template-free 3D cross-linked conducting polymer composite materials and highlights the potential of PPy-CoO MPCs as an efficient, low-cost, and viable solution for advanced small-scale, flexible energy storage systems.

Results and discussion

The synthesis of a three-dimensional polypyrrole soft gel was successfully achieved by a one-step, scalable, bicontinuous microemulsion (BME) polymerization technique. A schematic representation of the process is shown in Fig. 1. The bicontinuous microemulsion was formed in a nonionic nanoreactor composed of an intricate balance of water, oil, surfactant, and pyrrole monomer (Figure S1, *Supporting Information*). Nonionic surfactant system Triton X-100/n-butanol acts as a stabilizing agent, which reduces the interfacial tension, controls the dispersion of nanoparticles, and contributes to the uniform current distribution[28]. The Triton X-100 is well-known for its steric effect as a molecular spacer due to its phenyl ring[28,29]. This phenyl ring creates steric hindrance and increases the distance between molecules in a solution or within a matrix, which prevents

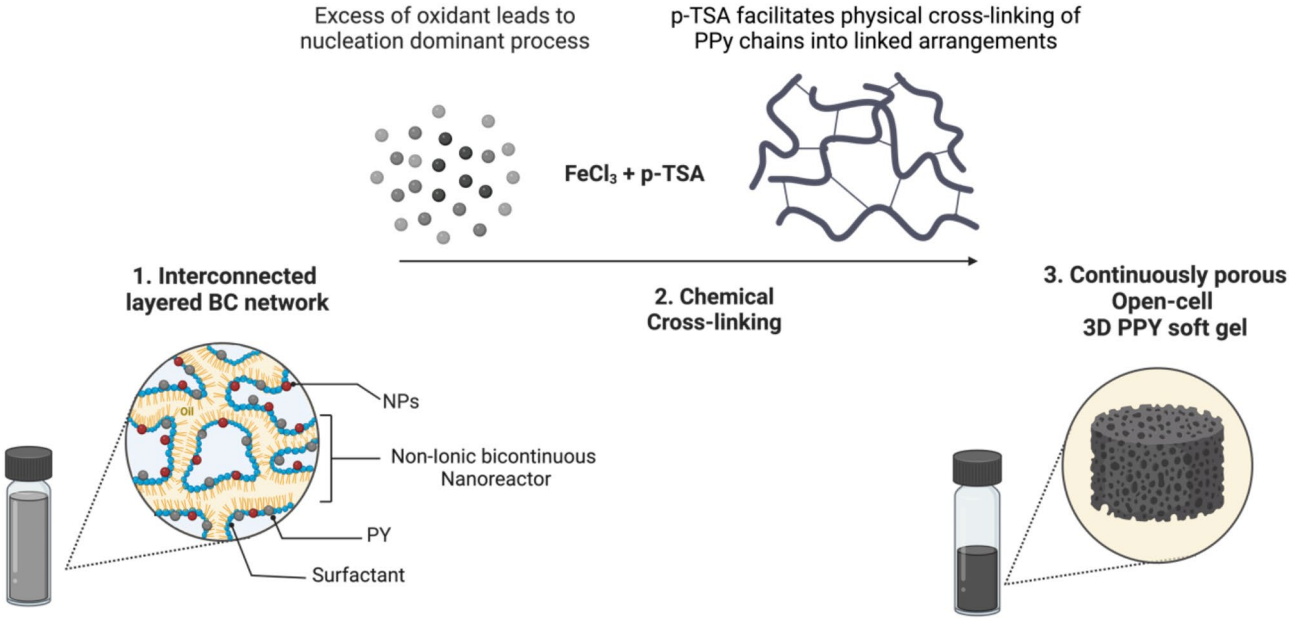

Fig. 1. Schematic representation of the self-templated 3D PPy soft gel formation.

aggregation of particles, as a result promoting better dispersion in a complex system[29–31]. This property allows controlled intermolecular packing, forming open structures with moderate porosity. The unique interpenetrated structure of microemulsion middle-phase (BME) is supported by the controlled separation of molecules by Triton X-100's steric effect, which leads to the formation of continuous pore networks. Tevi T. et al.[29] studied the effect of Triton X-100 on a double-layer capacitance of PEDOT: PSS films and concluded that the addition of Triton X-100 resulted in an increased storage capacity and stability, proving that the surfactant accelerated the ion transport. Also, they confirmed that nonionic surfactant opened gaps and formed porous morphology within the polymer film. Although the charge effect of surfactant on the capacitance of the material is still unclear, we chose nonionic surfactant to minimize any possible effect on charge density and ion mobility of composite material.

In our nanoreactor, monomer molecules were evenly distributed among all layers, which allowed a uniform initiation of the polymerization process after adding the oxidant solution, forming a 3D interconnected network. The formation of the continuously porous morphology is assisted not only by surfactant molecules but also by p-toluenesulfonic acid (p-TSA) which facilitates the cross-linking of polymers due to its cross-linking catalytic activity[32].

Previous studies have shown that an excess of oxidant molecules in BME promotes a nucleation-dominated process due to the multiple polymerization initiation points leading to the formation of polypyrrole nanoparticles rather than long chains[27].

The cross-linking of polypyrrole nanoparticles within bicontinuous microemulsion is attributed to several interactions due to the high amount of dopant and surfactant molecules in the reactor. Bicontinuous microemulsion (BME) serves as a unique template that facilitates the formation of a 3D cross-linked polypyrrole soft gel[33,34]. It is characterized by a specific, continuously interpenetrating network of oil and water stabilized by surfactant molecules. This microemulsion environment allows controlled polymerization of conducting polymers at the oil-water interface. We studied the cross-linking ability of pyrrole monomer due to its chemical stability, processability, flexibility, biocompatibility, and doping flexibility[35]. In a bicontinuous nonionic nanoreactor, pyrrole monomer was dissolved in the oil phase and oxidized by iron chloride ($FeCl_3$) oxidant doped with p-TSA. The localized polymerization at the interphase of two interpenetrated phases promotes the formation of polypyrrole chains that are spatially confined, closely packaged, and continuously porous.

The self-assembly of the polymer network is substantially facilitated by the strong π-π stacking interactions between pyrrole rings, which are specific to aromatic polypyrrole chains. Moreover, continued conjugation in polypyrrole amplifies π-π interactions by enhancing π-electron overlap, hence intensifying the interaction. The presence of a doping agent in the system facilitates the formation of hydrogen bonding between polypyrrole and the functional group of a doping molecule, which influences the 3D network stabilization and serves as a secondary cross-linking point. Furthermore, the microemulsion stabilized by nonionic surfactant molecules facilitates Van der Waals forces and electrostatic interactions between polypyrrole chains and other components. The combination of these interaction forces acts as a self-cross-linker, affecting the arrangement of polymer structure and its properties.

The rapidly nucleated polypyrrole nanoparticles tend to aggregate quickly. The synergistic effect of Triton X-100 and p-TSA does not allow the complete collapse of nanoparticles due to the increased electrostatic repulsion between growing PPy chains, leading to a cross-linked network with gaps and creating more open and interconnected porosity. It was observed that the higher concentrations of p-TSA lead to smaller, more stable microdomains, resulting in better control over particle nucleation and growth. This stabilized control allows more uniform particle size distribution and, consequently, a more homogeneous porous structure. As a dopant, p-TSA introduces sulfonate anions into the polymer structure, which helps to maintain the electrical conductivity of polypyrrole and its composites[36]. Several studies confirmed the superior electrical conductivity of PPy doped with p-TSA comparatively to other dopants due to a large number of negative charges on the dopant ion[37–39].

Experimental findings revealed that reactor composition, oil-to-monomer ratio, and oxidant concentration significantly influence the degree of cross-linking and porosity of the resultant material. We systematically analyzed several reactor compositions, as illustrated in Figure S2, Table S1, *Supporting Information*. The optimal composition for the reactor was found to be 50:20:30 (oil: water: surfactant). As was observed in our previous work, higher surfactant concentrations lead to the formation of layered morphology in polypyrrole[27]. We can obtain either layered nanosheets or porous microstructures depending on the oxidant concentration. Various oil-to-monomer ratios were examined and found that the 80:20 wt% ratio is the most favorable, exhibiting superior electrical and capacitive properties due to a well-interconnected network that promotes efficient charge transport within the gel matrix through optimal cross-linking (Figure S3, *Supporting Information)*. Generally, open-cell, continuously porous materials exhibit a high surface area, pore volume, and an interconnected pore structure that allows efficient fluid flow and mass transfer, making these materials ideal for the applications required for electrochemical reactions with better charge diffusion[7,40]. The actual images of the fabricated soft gels with evident open-cell porosity are demonstrated in Figure S4, *Supporting Information*. This open-cell structure also offers enhanced mechanical characteristics, including flexibility and better absorption. The unique composition of open microstructures provides a mixture of exceptional functionality and effectiveness, making them adaptable and desirable in a wide range of industrial and biological applications[7]. For these purposes, the functional nanoparticles of cobalt oxide (CoO) were introduced to the polymer soft gel, which served as a supporting matrix to endow the resulting composite material with multifunctional and tunable properties.

The morphology and microstructure characterizations of obtained 3D PPy-CoO soft gels were analyzed by Scanning Electron Microscopy (SEM) and Transmission Electron Microscopy (TEM) methods. As shown in Fig. 2, SEM images revealed the continuously porous nature of the polymer soft gels of pure PPy and PPy-CoO (0.5 wt%, 1.0 wt%, and 3.0 wt%).

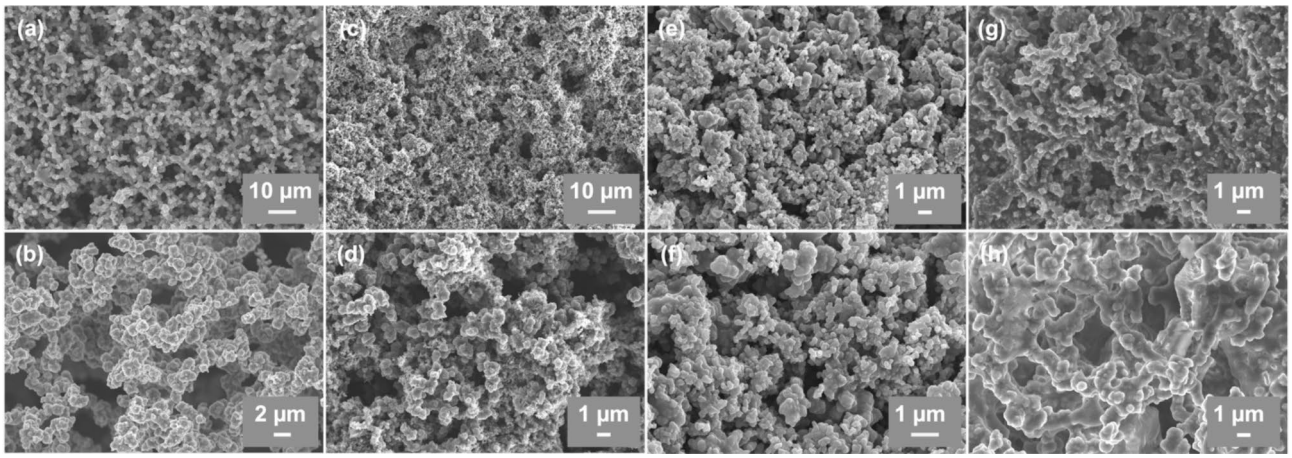

Fig. 2. SEM images of Pure PPy and PPy-CoO soft gels synthesized in bicontinuous nonionic nanoreactor showing continuously porous morphology of the polymer: (**a**, **b**) Pure PPy; (**c**, **d**) PPy-CoO 0.5 wt%; (**e**, **f**) PPy-CoO 1.0wt%; (**g**, **h**) PPy-CoO 3.0 wt%.

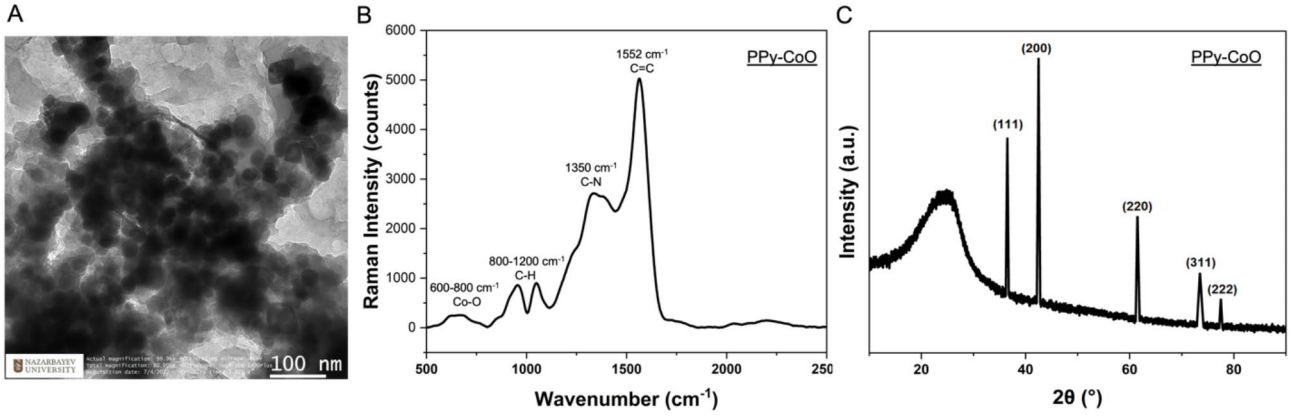

Fig. 3. TEM image of PPy-CoO 1.0 wt%; **B**) Raman Spectra of PPy-CoO 1.0 wt%; **C**) XRD Spectra of PPy-CoO 1.0 wt%.

FTIR spectra of the pure 3D PPy-CoO soft gels showed characteristic peaks of polypyrrole at 1547 cm^{-1} and 1456 cm^{-1} corresponding to the C = C/C-C stretching vibrations in the fundamental polypyrrole ring, indicating conductive nature of PPy (Figure S5A, *Supporting Information*)[13,35]. Additional peaks at 1235 and 1359 cm^{-1} indicate the C-N stretching vibration, while the peak at 1030 cm^{-1} reveals the O = S = O stretching, confirming the interaction with the p-TSA dopant[36]. A shift in the C-H in-plane bending vibration to 956 cm^{-1} and C = C stretching vibrations of the PPy ring to 1630 cm^{-1} indicates the dynamic response to the Co-O metal oxide within the composite structure[17,18]. The presence of the cobalt oxide nanoparticles in the polymer matrix was also proved in the elemental mapping images by the EDS technique shown in Figure S5B, *Supporting Information*. The thermogravimetric analysis (TGA) demonstrated the enhanced thermal stability for composite gel compared to pure polypyrrole, attributed to the thermal barrier effect of CoO particles, which delays the thermal degradation of the polypyrrole matrix. This stabilization of polymer chains is likely due to the interaction of polypyrrole with cobalt oxide and the formation of protective layers, which result in higher resistance to thermal decomposition (Figure S5C, *Supporting Information*)[18]. The TEM image in Fig. 3A further confirmed the structural integration of CoO nanoparticles into the polypyrrole.

Raman spectroscopy further verified the presence of a conjugated backbone of polypyrrole, with a strong peak at 1552 cm^{-1} attributed to C = C stretching (Fig. 3B). Peaks between 600 cm^{-1} to 800 cm^{-1} correspond to Co-O stretching vibrations, confirming the successful incorporation of cobalt oxide NPs into the polymer matrix. Overlapping peaks in 800 cm^{-1} to 1200 cm^{-1} range were attributed to stretching modes of PPy rings and C-H in-plane vibrations, with additional peaks between 1250 cm^{-1} and 1400 cm^{-1} corresponding to C-N stretching and C-H bending modes. The well-defined peaks suggest effective dispersion and interaction between the polypyrrole and cobalt oxide components. All defined peaks correspond with the reported literature values[41,42]. XRD analysis revealed the distinct peaks at 2θ values of approximately 36.5°, 42.5°, 61.5°, 74.5°, and 78.5° corresponding to the (111), (200), (220), (311), and (222) planes of crystalline CoO (Fig. 3C)[17,43,44]. These

sharp peaks, in combination with the broad polypyrrole feature, confirm the coexistence of crystalline cobalt oxide and the amorphous or semicrystalline nature of polypyrrole within the composite, which is essential for its catalytic and electronic applications. The swelling behavior of obtained polypyrrole soft gels were studied by water contact angle measurements where water droplets were immediately absorbed upon contact with the surface of a material Figure S6A, *Supporting Information*. Among different samples, a 3D PPy gel with an oil-to-water ratio of 50:20 demonstrated the highest swelling capacity, reaching 704% in water within 2 h. (Figure S6B, *Supporting Information*). Such good swelling performance can be attributed to the high crosslinking density of the polymer network and the effect of the doping agent contributing to the hydrophilicity and porosity of PPy soft gel, indicating better penetration of electrolytes into the polymer matrix[29,36]. The surface area of the synthesized pure polypyrrole gel was 12.4 m^2g^{-1}, consistent with microemulsion-formed materials, which are expected to be micro- and mesoporous[45]. The "micro-mesoporous" materials are preferable for micro-scale energy storage devices for optimal ion diffusion and surface area exposure[46]. A critical parameter, the pore volume of pure PPy was 0.064 cm^3g^{-1}, and the pore radius Dv(r) was 17 Å, indicating significant fluid and gas storage capacity. These characteristics place the polypyrrole gel within moderate surface area materials, typically ranging from 1 to 100 m^2g^{-1}, common for many polymers[7,9,47]. However, the presence of CoO NPs reduces the surface area and pore volume as the particles occupy available spaces within the polymer network (PPy-CoO 1.0wt%: S_{BET} 9.5 m^2g^{-1}, pore volume 0.029 cm^3g^{-1}, pore radius 17 Å). It was found that overloading the pores with metal oxides decreases the device's overall capacitance[48,49]. Maximum charge storage is achieved when the pore diameter matches the electrolyte ion size, as this maximizes ion accessibility[47]. Pore sizes that are either too small or too large lead to a significant drop in capacitance by limiting the surface interactions.

In this work, we hypothesized that the combined advantages of PPy-CoO soft gels, where PPy is a typical pseudo-capacitive p-type semiconductor, and CoO is a transition metal oxide p-type semiconductor, will synergistically enhance the energy storage and areal capacitance of overall micro-pseudocapacitor (MPC) performance. To find the optimal concentration of cobalt oxide, we studied three concentrations of NPs such as 0.5 wt%, 1.0 wt%, and 3.0 wt%. The CV curves are shown in Figure S7, *Supporting Information*. According to the results, the best capacitance was obtained by a sample with 1.0 wt% of CoO NPs. The rest of the measurements were done using this ratio.

The MPC device fabrication process is demonstrated in Fig. 4. To make an active material slurry, PVDF was dissolved in NMP and mixed with PPy-CoO and acetylene black powder. The viscosity of the resulting slurry was controlled by carefully adding of NMP droplets. The obtained slurry was cast on the PET substrate coated with a Cr (10 nm)/Au (100 nm) current collector layer. The dried electrode was etched by laser according to a specific design pattern. The final electrode was then coated with PVA/H_2SO_4 gel electrolyte. The co-planar interdigital architecture of the developed MPC was selected due to the better interaction of electrodes with electrolytes and high electrochemical surface area[50]. The surface morphology of the prepared electrode was examined using SEM, which confirmed the retention of its porous structure and the presence of CoO in the

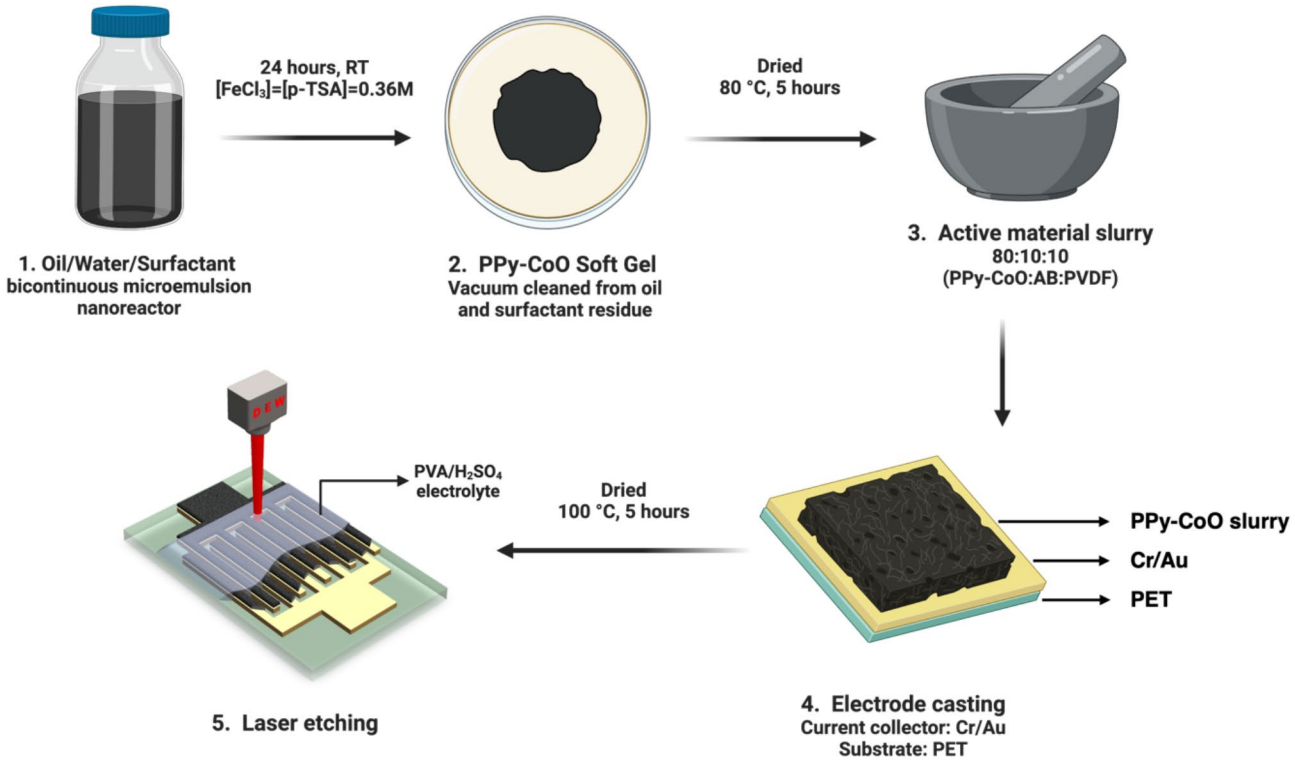

Fig. 4. The schematic illustration of PPy-CoO-based micro-pseudocapacitor fabrication.

electrode structure (Fig. 5). The width of the electrode interdigit was 452.2 ± 2.3 µm ($n = 5$), the interspace was 320 ± 4.2 µm ($n = 5$), and the thickness of the cast electrode was 32 ± 1.8 ($n = 5$) µm.

Electrochemical performance of the flexible PPy-CoO MPCs.

The electrochemical performance of the flexible PPy-CoO MPC device was evaluated using cyclic voltammetry (CV), electrical impedance spectroscopy (EIS), and galvanostatic charge-discharge (GCD) measurements in a two-electrode system with PVA/H_2SO_4 gel electrolyte. Figure 6 **(A, B, D, E)** shows the CV curves of pure PPy and composite PPy-CoO electrodes at different scan rates from 5 to 1000 mV s^{-1}. The CV curves of both devices exhibit a quasi-rectangular shape and demonstrate well-defined pseudocapacitive behavior, with notable differences in magnitude. The pure PPy electrode displays a broad CV curve with a relatively symmetrical current response across a wide voltage range. This is typical for conducting polymers that store charge through a continuous doping and dedoping process[11,13,16]. The wide shape of the curves reflects the ability of polypyrrole electrodes to store a charge across a broad range of potential windows, combining both redox pseudocapacitance and electron double-layer capacitance (EDLC). The areal capacitance of pure PPy electrode at 5 mV s^{-1} was 9.2 mF cm^{-2}, with energy and power densities of 1.28 µWh cm^{-2} and 22.99 µW cm^{-2}.

In contrast, despite a significant increase in capacitance and energy storage parameters, the PPy-CoO composite showed CV curves with more distinct profiles. At 5 mV s^{-1} the areal capacitance increased to 30.39 mF cm^{-2}. The energy and power densities reached 4.22 µWh cm^{-2} and 75.97 µW cm^{-2}, which is almost 3.5 times higher than pristine PPy electrode results. This enhanced capacitance is attributed to the additional charge storage capacity introduced by cobalt oxide through its localized Co^{2+}/Co^{3+} reversible redox reactions in a more defined voltage range[17]. CoO introduces Faradaic reactions, facilitated by proton (H^+) intercalation and deintercalation during charging and discharging into the electrode material:

$$CoO + H^+ \leftrightarrow Co^{3+} + OH^- + e^- \ (Oxidation\ Co^{2+}\ to\ Co^{3+}) \quad (1)$$

$$Co^{3+} + OH^- + e^- \leftrightarrow CoO + H^+ \ (Reduction\ Co^{3+}\ to\ Co^{2+}) \quad (2)$$

These redox reactions elevate the pseudocapacitive behavior and contribute to the overall enhanced capacitance and energy storage of the PPy-CoO device. The GCD curves obtained from both electrodes are nearly triangular at lower current densities, indicating capacitive behavior, but at higher current densities, we see the deviation from the shape due to the limitations of ion transport and the electrode's ability to maintain high currents (Fig. 6C, F). Comparatively, the higher charger-discharge time of PPy-CoO MPC suggests better capacitance even at higher current densities. The areal capacitance at 0.2 mA cm^{-2} was calculated for pure PPy MPC as 7.48 mF cm^{-2}, while PPy-CoO showed 30.58 mF cm^{-2}. The summary of all electrochemical measurements is presented in Table S2 and S3, *Supporting Information*. The EIS plot of PPy-CoO MPC shows the impedance

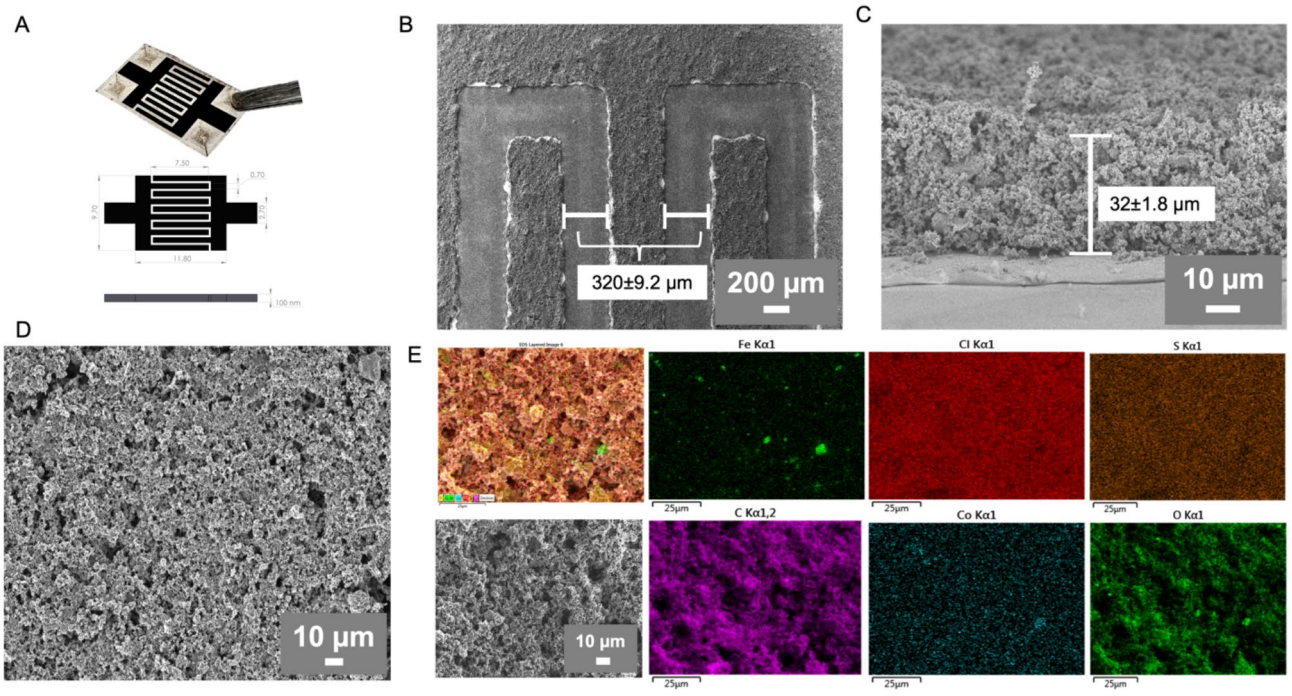

Fig. 5. (**A**) Actual image of PPy-CoO MPC with scale bar; (**B**) SEM image of electrode interdigit indicating the interspace between digits around 320 µm; (**C**) SEM image of electrode cross-section showing the thickness of electrode around 32 µm; (**D**) SEM image of electrode's surface morphology; (**E**) Elemental mapping of PPy-CoO electrode.

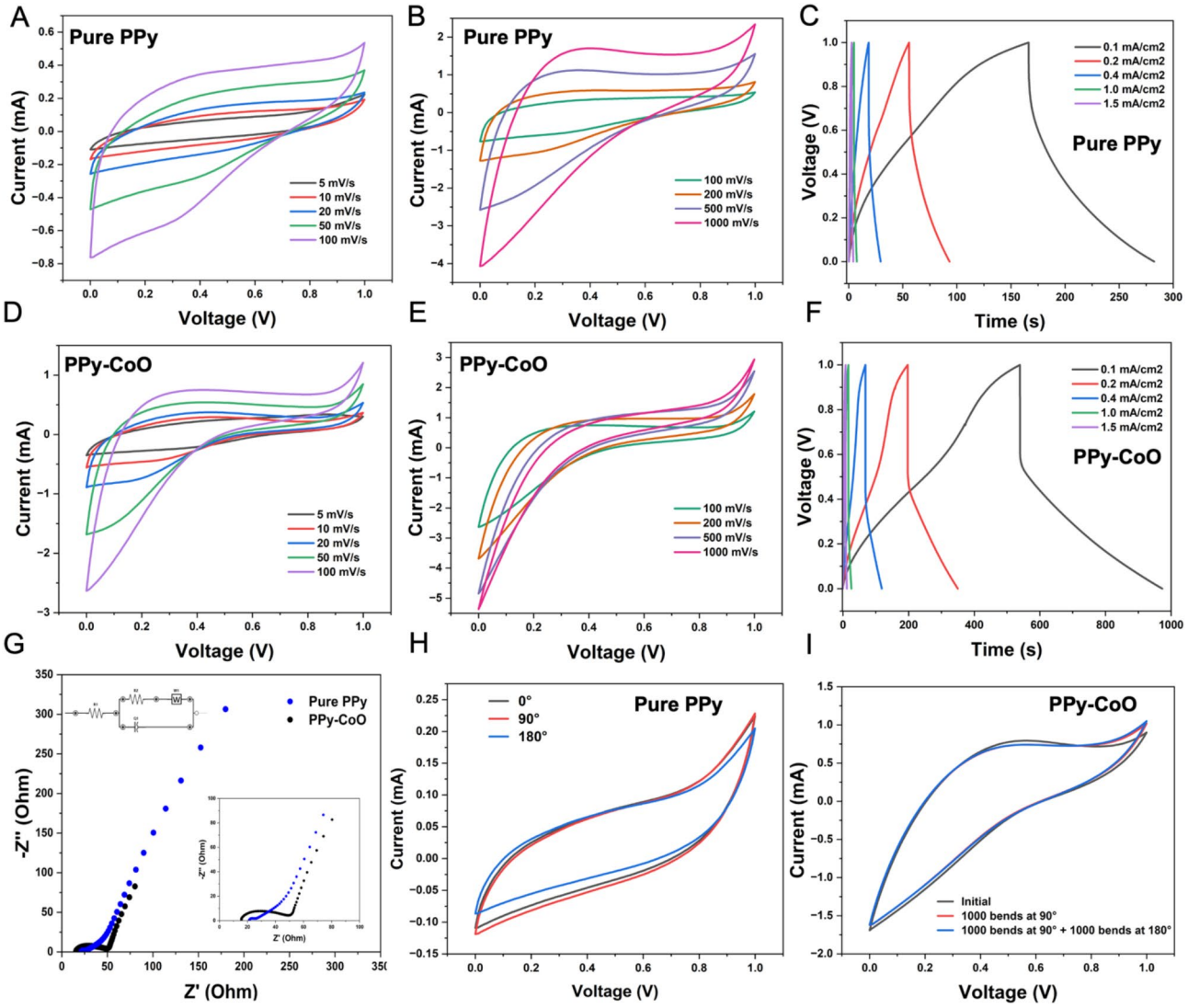

Fig. 6. **A** and **B**) CV curves of Pure PPy and PPy-CoO MPCs at scan rates (5 to 100 mV s^{-}); **C**) GCD curve of Pure PPy at different current densities; **D** and **E**) CV curves of Pure PPy and PPy-CoO MPCs at scan rates (100 to 1000 mV s^{-}); F) GCD curve of Pure PPy at different current densities; **G**) EIS plot of Pure PPy and PPy-CoO MPCs; **H**) CV curves of bent Pure PPy MPC at angles of 0°, 90°, and 180°. **I**) Mechanical and cycling stability of PPy-CoO MPC after 1000 bending cycles at 90° followed by an additional 1000 bending cycles at 180°.

characteristics of the device, with a larger semi-circle indicating charge transfer resistance and diffusion limitations compared to Pure PPy due to the lower pore volume of composite electrode occupied with CoO NPs (Fig. 6G). The sloping line at intermediate frequencies indicates the diffusion-controlled process, which results in efficient diffusion into the porous structure of the electrode material. The lower impedance of the Pure PPy is attributed to the better conductivity of polypyrrole due to the absence of insulating CoO NPs. Despite the slower ion diffusion in a composite material, it shows improved electrochemical stability. The devices were tested at three bending angles: 0°, 90°, and 180°. Both electrodes showed increased capacitance at a bending angle of 90°, with capacitance increasing slightly to 104% for Pure PPy and 106% for PPy-CoO, respectively. However, at more extreme bending angles, both devices exhibited a decrease in capacitance retention, likely due to structural changes in the electrode films. Despite this reduction, the PPy-CoO electrode outperformed Pure PPy, maintaining 95% capacitance retention after bending at 180°.

The mechanical stability of the device was further evaluated using cyclic voltammetry during bending cycles. (Fig. 6H and I) The PPy-CoO MPC was subjected to 1000 bending cycles at 90°, followed by an additional 1000 cycles at 180°. The capacitance retention of PPy-CoO MPC was 95.5% after first 1000 cycles at 90° and slightly improved to 96.2% after the additional 1000 cycles at 180°, highlighting the robust mechanical and electrochemical performance of the composite material.

We further evaluated the cycling stability of the device using GCD measurements after 10,000 cycles at a current density of 1 mA cm^{-2}. The PPy-CoO MPC demonstrated impressive performance, retaining 80% of its initial capacitance in the flat state, compared to only 30% for the pure PPy MPC (Fig. 7A, B). Remarkably, the

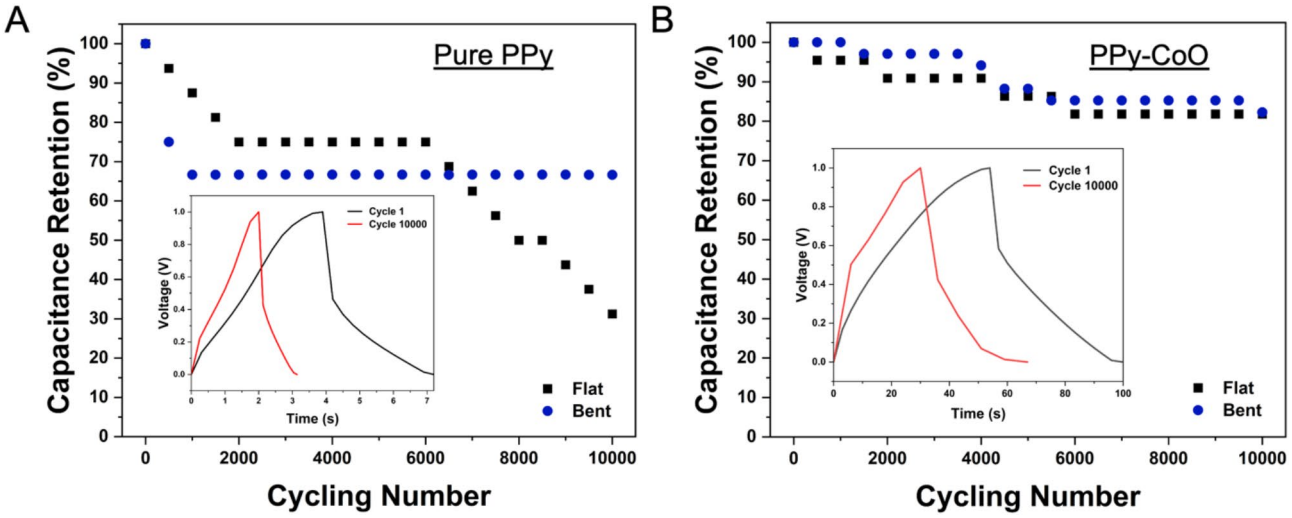

Fig. 7. **A** and **B**) Capacitance retention GCD profiles of Pure PPy MPC and PPy-CoO MPC at flat and bending positions at different angles after 10,000 cycles.

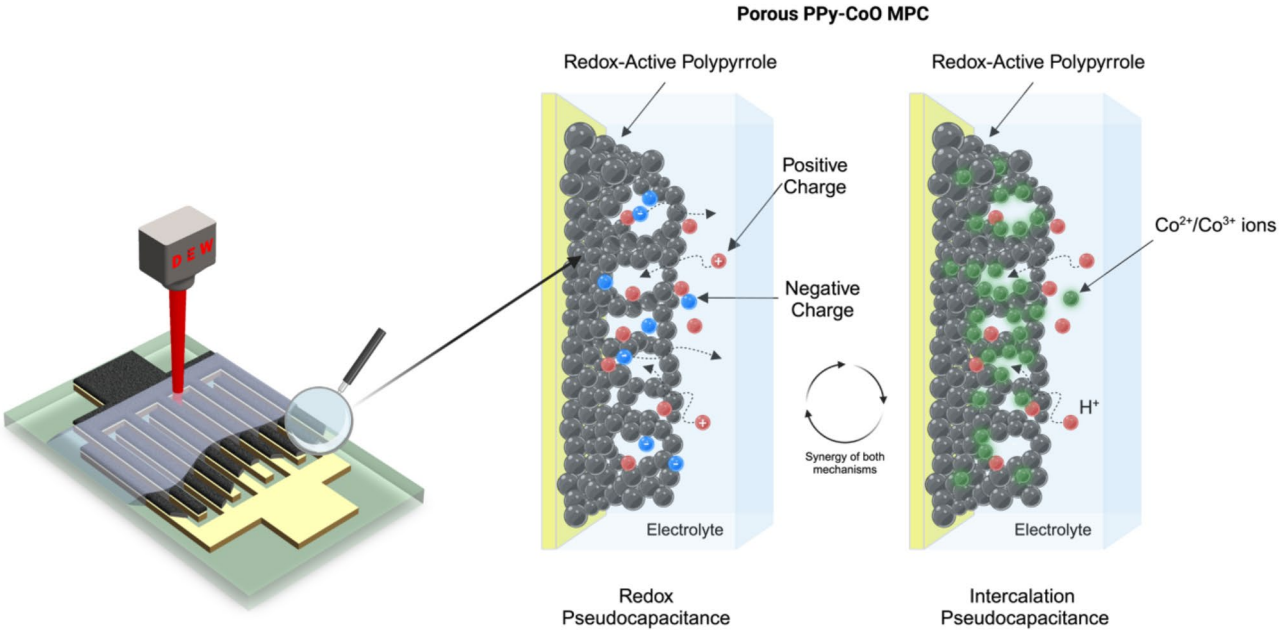

Fig. 8. Graphical illustration of suggested pseudocapacitance mechanism of fabricated PPy-CoO electrode for MPCs.

bent PPy-CoO device at a 180° angle retained 83% of its capacitance after 10,000 cycles, showcasing even better efficiency than in the flat state. Similarly, the Pure PPy MPC exhibited an improvement in capacitance retention at the bent state, increasing to 70%. This enhancement can be attributed to the reduced charge transfer distance under bending conditions. The incorporation of CoO into the polymer matrix not only significantly enhances capacitance but also greatly improves the long-term durability of the fabricated device. These results underscore the superior cycling stability of the PPy-CoO MPC, even under mechanical deformation at a bent angle of 180°.

The comparison of the obtained results with other micro-pseudocapacitors can be found in Table S4, *Supporting Information*.

The electrochemical mechanism observed in composite PPy-CoO electrodes can be explained by the synergistic interaction of PPy and CoO that enhances performance of the composite MPC. (Fig. 8) Polypyrrole as a conductive matrix provides rapid electron transport and continuous charge storage through surface redox reactions. Cobalt oxide is responsible for reversible redox reaction and intercalation pseudocapacitance since protons from the PVA/H_2SO_4 electrolyte intercalate into the tunnels or interlayers of redox-active composite

material. Despite the narrowed CV curves of the PPy-CoO electrode, the increase in capacitance and energy density is a result of these localized redox reactions.

Conclusion

A flexible solid-state micro-pseudocapacitors (MPCs) with outstanding areal capacitance (30.56 mF cm^{-2} at 0.2 mA cm^{-2}), impressive energy density (4.24 μWh cm^{-2}), and power density (75.97 μW cm^{-2}), remarkable flexibility and cycling stability (80% after 10 000 cycles) was achieved by the synergistic effect of interactions between polypyrrole (PPy) and cobalt oxide (CoO) NPs fabricated using one-step bicontinuous microemulsion (BME) polymerization technique. The comparative analysis shows the outperformance of the PPy-CoO MPC device over Pure PPy MPC. The unique morphology of interconnected nonionic bicontinuous microemulsion nanoreactors in combination with p-TSA, enabled the fabrication of self-assembled open-cell continuously porous conducting polymer composite for the first time. The open-cell microstructure enhanced the ion diffusion that improved the electrochemical, mechanical performance, and durability of the fabricated devices. We concluded that these outstanding research findings demonstrate the significant promise of fabricated material as an efficient electrode for micro-scale energy storage systems and other smart devices as well as the great potential of the proposed synthesis technique as an alternative to complicated and expensive conventional methods for porous CPs.

Methods

Materials

Pyrrole (≥ 98%, Sigma-Aldrich), cyclohexane (≥ 99%, Sigma-Aldrich), Triton X-100 (Sigma-Aldrich), n-butanol (99.8%, Sigma-Aldrich), anhydrous iron (III) chloride ($FeCl_3$, Sigma-Aldrich), p-Toluene sulfonic acid monohydrate (p-TSA, ≥ 99%, Sigma-Aldrich), and cobalt (II) oxide (CoO, Sigma-Aldrich). Pyrrole was purified by an aluminum oxide column before use.

Poly(vinyl alcohol) (PVA, M_w 89,000–98,000, Sigma-Aldrich), sulfuric acid (95–98%, Sigma-Aldrich), Poly(vinylidene difluoride) (PVDF, ≥ 86%, Sigma-Aldrich), *N*-Methyl-2-pyrrolidone (NMP, 99.5%, Sigma-Aldrich), acetylene black.

Synthesis of 3D continuously porous PPy-CoO soft gel

A nonionic nanoreactor containing a 50:20:30 ratio of cyclohexane/water/triton X-100@n-butanol was used to form a bicontinuous microemulsion (BME) for the synthesis of PPy-CoO soft gel[27,51]. The ternary phase diagram can be found in Figure S1, *Supporting Information*. The Oil-to-Monomer ratio (Cyclohexane: Py) was maintained at 80:20 wt%, and different concentrations of CoO (0.5 wt%, 1.0 wt%, and 3 wt%) were mixed with pyrrole monomer at the beginning of the reaction. To prepare the BME, 34.2 ml of cyclohexane, 6.9 ml of pyrrole with CoO, 21.6 ml of surfactant solution (triton X-100@n-butanol), and 13.3 ml of oxidant solution containing 0.36 M $FeCl_3$, and 0.36 M p-TSA were mixed and left to stabilize for 24 h. The reactor components can be easily adjusted to scale up the synthesis from small vials to larger bottles. To initiate polymerization, the aqueous solution must be added at the end. The obtained gel was purified by vigorously rinsing it with acetone and deionized (DI) water under vacuum filtration and then dried in a vacuum oven at 80 °C for 5 h.

Fabrication of PPy-CoO micro-pseudocapacitor (MPC)

The electrode was prepared using a slurry casting method. The slurry is composed of 80 wt% of active material (either pure PPy or PPy-CoO composite), 10 wt% of acetylene black, and 10 wt% of PVDF, with ≤ 1 ml of NMP based on the total mass of the active material. The prepared slurry was cast on the PET/Cr/Au substrate by a doctor blade with a thickness of 30 μm and dried under vacuum at 100 °C for 5 h. The dried electrode was etched using a Power Supply Laser Module (GTDC 2425) following the designed pattern, which can be found in Figure S8, *Supporting Information*.

The obtained MPC was coated by gel electrolyte and dried at room temperature overnight. The PVA/H_2SO_4 gel electrolyte was prepared by dissolving 1 g of PVA in 10 ml of deionized water and stirring the mixture for 2 h at 95 °C until the PVA was fully dissolved. After cooling, 1 g of sulfuric acid was added, and the solution was stirred overnight.

Characterization of PPy-CoO soft gel

Scanning electron microscopy (SEM, ZEISS Crossbeam 540) and transmission electron microscopy (TEM, JEOL JEM-1400 Plus) were used to examine the surface morphology and structure of samples. The Horiba LabRam Evolution spectrometer recorded Raman spectra. The Fourier transform infrared (FTIR) spectra were obtained by the Nicolet iS10 spectrometer. The X-ray diffraction (XRD) study was conducted using a SmartLab (Rigaku) high-resolution X-ray diffractometer. TGA data was collected from the Simultaneous Thermal Analyzer (STA) 6000. BET surface area, pore volume, and size measurements were obtained by a nitrogen porosimeter (Autosorb IQ, Anton Paar).

Electrochemical tests of micro-pseudocapacitors (MPCs)

Cyclic voltammetry (CV), galvanostatic charge/discharge (GCD), and electrochemical impedance spectroscopy (EIS) techniques were used to investigate the electrochemical performance of MPCs. All tests were performed by PalmSens4 potentiostat/galvanostat. The CV measurements were carried out within a potential window of 0–1 V, with scan rates ranging from 5 to 1000 mV s^{-1}, while GCD tests were performed at current densities ranging from 0.1 to 1.5 mA cm^{-2}. EIS was performed over a frequency range of 200 kHz to 0.1 Hz, with a voltage amplitude of 10 mV.

The actual capacitance of the device was calculated according to the following equations:[52].
From CV curves:

$$C = \frac{\int_{V_i}^{V_f} idV}{2 \times \vartheta \times \Delta V} \tag{4}$$

From charge-discharge curves:

$$C = \frac{I \times \Delta t}{\Delta V} \tag{5}$$

Where $\int_{V_i}^{V_f} idV$ is the area of the CV curve, ϑ is the voltage scan rate (V s^{-1}), ΔV is the potential window, I is the current used for charging and discharging (A) and Δt is the discharge time (s).

The energy density (E, in mWh cm^{-2}) and power density (P, in mW cm^{-2}) of the device were calculated using the following equations[52]:

$$E = \frac{C}{2 \times 3600} \tag{6}$$

$$P = \frac{3600 \times E \times \vartheta}{V} = \frac{3600 \times E}{\Delta t} \tag{7}$$

The capacitance retention of the device was evaluated by calculating the ratio of the specific areal capacitance at each cycle to the specific areal capacitance measured in the first cycle. This evaluation was carried out over 10,000 cycles at the current density of 1 mA cm^{-2}.

Data availability

Data is provided within the manuscript and supplementary information files. Supplementary information accompanies this paper at http://www.nature.com/ scientificreports.

Received: 29 November 2024; Accepted: 7 March 2025
Published online: 20 March 2025

References

1. Li, L., Wu, Z., Yuan, S. & Zhang, X. B. Advances and challenges for flexible energy storage and conversion devices and systems. *Energy and Environmental Science* vol. 7 2101–2122 Preprint at (2014). https://doi.org/10.1039/c4ee00318g
2. Genene, Z., Xia, Z., Yang, G., Mammo, W. & Wang, E. Recent Advances in the Synthesis of Conjugated Polymers for Supercapacitors. *Advanced Materials Technologies* vol. 9 Preprint at (2024). https://doi.org/10.1002/admt.202300167
3. Wang, W. et al. Flexible supercapacitors based on stretchable conducting polymer electrodes. *Polym. (Basel)* **15**, (2023).
4. Zhang, X. et al. In-plane flexible solid-state microsupercapacitors for on-chip electronics. *Energy* **170**, 338–348 (2019).
5. Bi, S., Cao, H., Wang, R., Wan, F. & Niu, Z. In-plane micro-sized energy storage devices: from device fabrication to integration and intelligent designs. *J. Energy Chem.* **63**, 25–39 (2021).
6. Xu, Y. et al. Recent progress in electrode materials for micro-supercapacitors. *iScience* vol. 27 Preprint at (2024). https://doi.org/10.1016/j.isci.2024.108786
7. Han, J., Johnson, I. & Chen, M. 3D Continuously Porous Graphene for Energy Applications. *Advanced Materials* vol. 34 Preprint at (2022). https://doi.org/10.1002/adma.202108750
8. Chu, X. et al. Conducting polymer ink for flexible and printable micro-supercapacitors with greatly-enhanced rate capability. *J. Power Sources* **513**, (2021).
9. Ham, H., Sim, G., Choi, W. & Park, M. J. Porous pathways: Exploring the future of conducting polymers. *Bulletin of the Korean Chemical Society* vol. 45 200–213 Preprint at (2024). https://doi.org/10.1002/bkcs.12814
10. Beidaghi, M. & Wang, C. Micro-supercapacitors based on three dimensional interdigital polypyrrole/C-MEMS electrodes. *Electrochim. Acta.* **56**, 9508–9514 (2011).
11. Li, P. et al. Flexible, long cycle-life micro-supercapacitor with polypyrrole@Ag-wall interdigitated electrodes fabricated by micro-3D printing and electrochemical polymerization. *J. Manuf. Process.* **94**, 338–347 (2023).
12. Zhao, Y. et al. Hierarchical polypyrrole@cobalt sulfide-based flexible on-chip microsupercapacitors with ultrahigh energy density for self-charging system. *Nano Res.* **16**, 555–563 (2023).
13. Qin, J. et al. Hierarchical ordered Dual-Mesoporous polypyrrole/graphene nanosheets as Bi-Functional active materials for High-Performance planar integrated system of Micro-Supercapacitor and gas sensor. *Adv. Funct. Mater.* **30**, (2020).
14. Ma, S. et al. Flexible planar microsupercapacitors based on polypyrrole nanotubes. *ACS Appl. Energy Mater.* **4**, 8857–8865 (2021).
15. Tahir, M. et al. Pushing the electrochemical performance limits of polypyrrole toward stable microelectronic devices. *Nanomicro Lett.* **15**, (2023).
16. Tao, J. et al. Solid-state high performance flexible supercapacitors based on polypyrrole-mno2-carbon fiber hybrid structure. *Sci. Rep.* **3**, (2013).
17. Kunhikrishnan, L. & Shanmugham, R. High electrochemical performance of morphologically controlled Cobalt oxide for supercapacitor application. *Mater. Charact.* **177**, (2021).
18. Wei, H. et al. Electropolymerized polypyrrole nanocomposites with Cobalt oxide coated on carbon paper for electrochemical energy storage. *Polym. (Guildf).* **67**, 192–199 (2015).
19. Lee, C. P. et al. Cobalt oxide-decorated silicon carbide nano-tree array electrode for micro-supercapacitor application. *Materials* **14**, (2021).
20. Haider, W. A. et al. Bilayered microelectrodes based on electrochemically deposited MnO2/polypyrrole towards fast charge transport kinetics for micro-supercapacitors. *RSC Adv.* **10**, 18245–18251 (2020).
21. Naderi, L. & Shahrokhian, S. Wire-type flexible micro-supercapacitor based on MOF-assisted sulfide nano-arrays on dendritic CuCoP and V2O5-polypyrrole/nanocellulose hydrogel. *Chem. Eng. J.* **476**, (2023).
22. Magazov, Y. et al. Copper oxide coupled with photon upconversion for solar water splitting. *Commun. Mater.* **5**, (2024).

23. Magazov, Y. et al. Photoelectrochemical water splitting using cuprous oxide (Cu2O)-Based Photocathode – A review. *ES Energy Environ.* https://doi.org/10.30919/esee1347 (2024).
24. Reddy, M. V., Prithvi, G., Loh, K. P. & Chowdari, B. V. R. Li storage and impedance spectroscopy studies on Co3O4, CoO, and CoN for Li-Ion batteries. *ACS Appl. Mater. Interfaces*. **6**, 680–690 (2014).
25. Zhou, C., Zhang, Y., Li, Y. & Liu, J. Construction of high-capacitance 3D CoO@Polypyrrole nanowire array electrode for aqueous asymmetric supercapacitor. *Nano Lett.* **13**, 2078–2085 (2013).
26. Zhu, Y. G., Wang, Y., Shi, Y., Wong, J. I. & Yang, H. Y. CoO nanoflowers woven by CNT network for high energy density flexible micro-supercapacitor. *Nano Energy*. **3**, 46–54 (2014).
27. Abutalip, M. et al. Strategic synthesis of 2D and 3D conducting polymers and derived nanocomposites. *Adv. Mater.* **35**, (2023).
28. Devaraj, S. & Munichandraiah, N. The effect of nonionic surfactant Triton X-100 during electrochemical deposition of MnO[sub 2] on its capacitance properties. *J. Electrochem. Soc.* **154**, A901 (2007).
29. Tevi, T., Birch, S., Thomas, S. W., Takshi, A. & S. W. & Effect of Triton X-100 on the double layer capacitance and conductivity of poly(3,4-ethylenedioxythiophene):poly(styrenesulfonate) (PEDOT:PSS) films. *Synth. Met.* **191**, 59–65 (2014).
30. Manda, A. B., Ray, S., Biswas, A. M. & Moulik, S. P. *Physicochemical studies on the characterization of Triton X 100 micelles in an aqueous environment and in the presence of additives*. *J. Phys. Chem.* vol. 84 (1980). https://pubs.acs.org/sharingguidelines
31. Nowok, A. et al. Phenyl ring: A steric hindrance or a source of different hydrogen bonding patterns in Self-Organizing systems?? *J. Phys. Chem. Lett.* **12**, 2142–2147 (2021).
32. Prince, L., Guggenberger, P., Santini, E., Kleitz, F. & Woodward, R. T. Metal-Free Hyper-Cross-Linked polymers from benzyl Methyl ethers: A route to polymerization catalyst recycling. *Macromolecules* **54**, 9217–9222 (2021).
33. Kawano, S., Kobayashi, D., Taguchi, S., Kunitake, M. & Nishimi, T. Construction of continuous porous organogels, hydrogels, and bicontinuous Organo/hydro hybrid gels from bicontinuous microemulsions. *Macromolecules* **43**, 473–479 (2010).
34. Sakata, K. et al. Continuous porous poly(N-isopropylacrylamide) gels prepared from a bicontinuous microemulsion. *Chem. Lett.* **43**, 240–242 (2014).
35. Wang, L. X., Li, X. G. & Yang, Y. L. *Preparation, properties and applications of polypyrroles*. *React. Funct. Polym.* vol. 47 (2001). www.elsevier.com/locate/react
36. Tian, F. et al. Spongy p-Toluenesulfonic Acid-doped polypyrrole with extraordinary rate performance as durable anodes of Sodium-Ion batteries at different temperatures. *Langmuir* **36**, 15075–15081 (2020).
37. Zhang, M. et al. Polypyrrole film based flexible supercapacitor: mechanistic insight into influence of acid dopants on electrochemical performance. *Electrochim. Acta*. **357**, 136877 (2020).
38. Goel, S., Mazumdar, N. A. & Gupta, A. Synthesis and characterization of polypyrrole nanofibers with different dopants. *Polym. Adv. Technol.* **21**, 205–210 (2010).
39. Zhang, W. D., Xiao, H. M., Zhu, L. P., Fu, S. Y. & Wan, M. X. Facile one-step synthesis of electromagnetic functionalized polypyrrole/Fe3O4 nanotubes via a self-assembly process. *J. Polym. Sci. Polym. Chem.* **48**, 320–326 (2010).
40. Liu, L., Kai, H., Nagamine, K., Ogawa, Y. & Nishizawa, M. Porous polymer microneedles with interconnecting microchannels for rapid fluid transport. *RSC Adv.* **6**, 48630–48635 (2016).
41. Liu, Y. C. & Hwang, B. J. Identification of oxidized polypyrrole on Raman spectrum. *Synth. Met.* **113**, 203–207 (2000).
42. Hasoon, S. & Salah Abdullah, H. Electrochemical polymerization and Raman study of polypyrrole and polyaniline thin films. *Article Int. J. Phys. Sci.* **7**, 5468–5476 (2012).
43. Anwar, A., Numan, A., Siddiqui, R. & Khalid, M. & Khan, N. A. Cobalt nanoparticles as novel nanotherapeutics against Acanthamoeba castellanii. *Parasit. Vectors* **12**, (2019).
44. Wang, D., Wang, Q. & Wang, T. Morphology-controllable synthesis of Cobalt oxalates and their conversion to mesoporous Co3O4 nanostructures for application in supercapacitors. *Inorg. Chem.* **50**, 6482–6492 (2011).
45. Luo, H. et al. Nanoarchitectured Porous Conducting Polymers: From Controlled Synthesis to Advanced Applications. *Advanced Materials* vol. 33 Preprint at (2021). https://doi.org/10.1002/adma.202007318
46. Li, L., Meng, J., Zhang, M., Liu, T. & Zhang, C. Recent advances in conductive polymer hydrogel composites and nanocomposites for flexible electrochemical supercapacitors. *Chem. Commun.* **58**, 185–207 (2022).
47. Zhang, L. L., Gu, Y. & Zhao, X. S. Advanced porous carbon electrodes for electrochemical capacitors. *J. Mater. Chem. Mater.* **1**, 9395–9408 (2013).
48. Huang, X., Kim, M., Suh, H. & Kim, I. Hierarchically nanostructured carbon-supported manganese oxide for high-performance pseudo-capacitors. *Korean J. Chem. Eng.* **33**, 2228–2234 (2016).
49. Saruhan, B., Gönüllü, Y. & Arndt, B. Pseudocapacitive and hierarchically ordered porous electrode materials supercapacitors. in Energy Harvesting and Storage: Materials, Devices, and Applications IV vol. 8728 872810 (SPIE, (2013).
50. Chu, X. et al. Air-Stable conductive polymer ink for printed wearable Micro-Supercapacitors. *Small* **17**, (2021).
51. Wang, B. et al. Properties of TX-100/n-butanol/cyclohexane/water microemulsion and its osmosis for wood. *J. Biobased Mater. Bioenergy*. **5**, 197–202 (2011).
52. Chaney, L. E., Hyun, W. J., Khalaj, M., Hui, J. & Hersam, M. C. Fully printed, High-Temperature Micro-Supercapacitor arrays enabled by a hexagonal Boron nitride ionogel electrolyte. *Adv. Mater.* https://doi.org/10.1002/adma.202305161 (2023).

Acknowledgements

The authors acknowledge the financial support from the Faculty-development Competitive Research Grants Program of Nazarbayev University for 2023-2025 (Project ref. no. 20122022FD4114), "Fabrication of Nanostructured Conducting Polymers and Their Nanocomposites for Energy Applications"; Ministry of Education and Science of the Republic of Kazakhstan under project No. BR21882439, "Advancement of the Green Energy: Foundational Research of Solar Fuel Technologies for Sustainable Production and Advanced Storage".

The scientific group also extends its gratitude to Dr. Aishuak Konarov and his lab members for supplying the required chemicals and to Dr. Batukhan Tatykayev for the use of the X-ray diffractometer.

Author contributions

N.N. conceived and supervised the research project. G.Z. developed the idea, conducted material synthesis experiments, materials characterization, fabricated electrodes, interpreted the data, and wrote the manuscript. V.K. developed the MPC design pattern, draw MPC illustrations. A.A. conducted the laser etching of the electrode and fabricated device, electrochemical measurements, analyzed data. Y.M. conducted XRD, Raman and SEM analysis. S.A. supervised synthesis of material.

Declarations

Competing interests
The authors declare no competing interests.

Additional information
Supplementary Information The online version contains supplementary material available at https://doi.org/10.1038/s41598-025-93663-5.

Correspondence and requests for materials should be addressed to N.N.

Reprints and permissions information is available at www.nature.com/reprints.

Publisher's note Springer Nature remains neutral with regard to jurisdictional claims in published maps and institutional affiliations.